Image decomposition using adaptive second-order total generalized variation

Jianlou Xu · Xiangchu Feng · Yan Hao · Yu Han

Abstract This paper proposes a new model for image decomposition which separates an image into a cartoon, consisting only of geometric objects, and an oscillatory component, consisting of textures or noise. The proposed model is given in a variational formulation with adaptive second-order total generalized variation (TGV). The adaptive behavior preserves the key features such as object boundaries and textures while avoiding staircasing effect. To speed up the computation, the split Bregman method is used to solve the proposed model. Experimental results and comparisons demonstrate the proposed model is more effective for image decomposition than the methods of the state-of-the-art image decomposition models.

Keywords Image decomposition · Cartoon · Texture · TGV · Split Bregman · Staircasing effect

1 Introduction

The task of decomposing a signal or an image into different components is of great interest in many applications. For instance, a prominent practical problem is represented by the separation of the speaker's voice from the background noise at a cocktail party. In general, a nature image contains geometric parts and textural parts. Image decomposition refers to the splitting of an image into two or more components. In particular, much of this progress has been made through the use of nonlinear partial differential equations to model oscillating patterns which represent texture or noise.

The general variational framework for decomposing image f into structure and texture is given in Meyer's models [1] as an energy minimization problem

$$\inf_{(u,v)\in X_1 \times X_2} F_1(u) + \lambda F_2(v), \text{ s.t. } f = u + v, \tag{1}$$

where F_1, $F_2 \geq 0$ and u, v denote the geometric parts (cartoon) and oscillatory parts (textures) of image f, respectively. The constant λ is a tuning parameter. It is a key to determine a good model that one can appropriately choose the space X_1, X_2 for cartoon u and texture v such that $F_1(u) \ll F_2(u)$ and $F_1(v) \gg F_2(v)$, such conditions would insure a clear cartoon + texture separation; In other words, if u is only cartoon, without texture, then texture components must be penalized by F_1, but not by F_2, and vice-versa.

In [1], Meyer introduces the notion that image denoising can be thought of as image decomposition for the application of texture extraction. Furthermore, he introduces a variant of the popular model by Rudin, Osher and Fatemi (ROF) [2] based on a space called the G space for this very purpose. The idea is to replace the L^2 norm in the ROF model with a weaker norm that better captures textures or oscillating patterns. However, in practice, the model is difficult to implement, so the authors in [3] suggest to overcome this difficulty using the following approximation model

J. Xu (✉) · X. Feng · Y. Hao · Y. Han
School of Sciences, Xidian University, 2 Tai Bai Road,
Xi'an 710071, Shaanxi, People's Republic of China
e-mail: xujianlou@126.com

X. Feng
e-mail: xcfeng@mail.xidian.edu.cn

Y. Han
e-mail: hany_xidian@126.com

J. Xu · Y. Hao
School of Mathematics and Statistics, Henan University of Science and Technology, 263, Kai Yuan Road, Luoyang 471023, Henan, People's Republic of China
e-mail: haoyan_@126.com

$$\inf_{u,g_1,g_2} \int_\Omega |\nabla u|\, \mathrm{d}x + \lambda \int_\Omega |f - u - \partial_x g_1 - \partial_y g_2|^2\, \mathrm{d}x$$

$$+ \mu \left[\int_\Omega \left(\sqrt{g_1^2 + g_2^2} \right)^p \mathrm{d}x \right]^{\frac{1}{p}}. \tag{2}$$

In a subsequent work, Osher, Sole and Vese (OSV) [4] let $p = 2$ and gave the another approximation model as follows.

$$\inf_u E(u) = \int_\Omega |\nabla u|\mathrm{d}x + \frac{\gamma}{2} \|f - u\|_{H^{-1}}^2. \tag{3}$$

The H^{-1} norm is defined as $\|f - u\|_{H^{-1}}^2 = \int_\Omega |\nabla (\Delta^{-1}) (f - u)|^2\, \mathrm{d}x$, and the definition of inverse Laplacian Δ^{-1} is in [4]. In the Euler-Lagrange variational framework, this energy minimized by the solution of the following fourth-order PDE:

$$\frac{\partial u}{\partial t} = -\Delta \left(\operatorname{div} \left(\frac{\nabla u}{|\nabla u|} \right) \right) + \gamma (f - u) \tag{4}$$

with the boundary condition mentioned in [4]. Numerical experiments show that the Eqs. (2) and (3) separate texture from the object better than the ROF model, especially the texture component contains much less cartoon information. Compared with Eq. (2), the Eq. (3) has few parameter, so it is easy to implement. However, a particular caveat of such TV regularization is the staircasing effect. Generally speaking, the staircasing effect severely impacts the quality of image denoising and decomposition. Thus, ameliorating the staircasing effect should be considered a priority in image decomposition problems.

There are many variational models about image denoising and decomposition [5–11], such as the adaptive TV determined by a threshold parameter given in advance [5]; however, the threshed parameter is difficult to be chosen; another way is that the higher-order variational model is introduced in [7], but the higher-order equation can make the image edges and texture blurry; though the non-convex model [9] can obtain the better results, it has not the global minimal solution.

Recently, a new mathematical framework of total generalized variation (TGV) is proposed by Bredies, Kunisch and Pock [12]. The main property of TGV regularization is that it allows to reconstruct piecewise polynomial functions of arbitrary order (piecewise constant, piecewise affine, piecewise quadratic, ...). As the TV regularizer, the TGV regularizer has the nice property of being convex, this allows to compute a globally optimal solution. Many good results have been obtained about TGV in [12–15].

In this paper, we propose a new image decomposition model based on the adaptive second-order TGV. In the new model, an edge indicator function is introduced to the second-order TGV. So the new model can take advantage of the

properties of the second-order TGV to extract the texture while reducing the noise; meanwhile, the edge indicator function can adaptively preserve the key features such as object boundaries. To solve the proposed model, the split Bregman method and primal-dual approach are used in the numerical algorithm. Experimental results show that the proposed model can achieve a better trade-off between noise removal and image decomposition while avoiding the staircase effect.

This paper is organized as follows. In Sect. 2, we briefly introduce the mathematical framework used in this paper. In Sect. 3, the proposed model and the corresponding algorithm are given. In Sect. 4, the numerical discrete method is discussed. In Sect. 5, some numerical experiments are given to test the proposed algorithm. At last, the conclusions are drawn out in Sect. 6.

2 Mathematical framework

This section is mainly devoted to the introduction of the definition of TGV and some of its basic properties [12–15].

Definition 1 Let $\Omega \subset R^d$ be a be a bounded domain, $k \geq 1$ and $\alpha_0, \ldots, \alpha_{k-1} > 0$. Then, the TGV of order k with weight α for $u \in L_{\mathrm{loc}}^1(\Omega)$ is defined as the value of the functional

$$\mathrm{TGV}_\alpha^k(u)$$

$$= \sup \left\{ \int_\Omega u \operatorname{div}^k \phi\, \mathrm{d}x : \phi \in C_c^k \left(\Omega, \operatorname{Sym}^k \left(R^d \right) \right), \right.$$

$$\left. \left\| \operatorname{div}^l \phi \right\|_\infty \leq \alpha_l,\ l = 0, \ldots, k-1 \right\}, \tag{5}$$

where $C_c^k \left(\Omega, \operatorname{Sym}^k \left(R^d \right) \right)$ and $\operatorname{Sym}^k \left(R^d \right)$ denote the space of continuously differentiable symmetric k-tensors and symmetric k-tensors in Ω, respectively. The l-divergence of a symmetric k-tensors field is a symmetric $(k-l)$-tensors field, which is given by $\left(\operatorname{div}^l v \right)_\beta = \sum_{v \in M_l} \frac{l!}{\gamma!} \frac{\partial^l v_{\beta+\gamma}}{\partial x^\gamma}$ for each component $\beta \in M_{k-l}$, where M_k are the multi-indices of order k, that is, $M_k = \left\{ \beta \in \mathbb{N}^d \left| \sum_{i=1}^d \beta_i = k \right. \right\}$.

Definition 2 The space $\mathrm{BGV}_\alpha^k(\Omega) = \left\{ u \in L^1(\Omega) \left| \mathrm{TGV}_\alpha^k(u) < \infty \right. \right\}$, equipped with the norm $\|u\|_{\mathrm{BGV}_\alpha^k} = \|u\|_1 + \mathrm{TGV}_a^k(u)$, is called the space of functions of bounded generalized variation of order k with weight α. In particular, when $k = 2$, $\mathrm{BGV}_\alpha^2(\Omega)$ coincides with the BV (Ω) (bounded variation space), in the topological sense.

From the above definition 1, we can see that when $k = 1$ and $\alpha = 1$, Eq. (5) corresponds to the dual definition of the TV semi-norm, that is, TGV is indeed a generalization

of the TV regularizer. Using the Legendre-Fenchel duality, the problem (5) can be transformed to its primal formulation [12]:

$$\text{TGV}_\alpha^k (u) =$$

$$\inf_{\substack{u_l \in C_c^{k-l}(\Omega, \text{Sym}^l(R^d)) \\ l=1,\dots,k-1,\, u_0=u,\, u_k=0}} \sum_{l=1}^{k} \alpha_{k-l} \int_\Omega |\varepsilon(u_{l-1}) - u_l|\, \mathrm{d}x, \quad (6)$$

where $\varepsilon(u_{l-1})$ denotes the symmetrized gradient operator

$$\varepsilon(u_{l-1}) = \frac{\nabla u_{l-1} + (\nabla u_{l-1})^T}{2}.$$

From Eqs. (5), (6), we can see that this representation has converted functional (5) which depends on higher-order derivatives into a functional of recursive expression depending only on first-order derivatives. Using this representation, one can intuitively assess how the TGV is working. That is, $\text{TGV}_\alpha^k(u)$ automatically balances the first- and higher-order derivatives instead of using any fixed combination. In particular, when $k = 2$, it corresponds to the second-order TGV. Different from the usual TV, TGV_α^2 as a regularizer does not lead to the staircasing effect. Moreover, TGV_α^2 has many good properties, such as it is proper, convex and lower semi-continuous on each $L^p(\Omega)$, $1 \le p < \infty$, and it is a semi-norm on $BV(\Omega)$, etc (see Ref. [12,13]). These properties have been widely applied to the image processing.

3 The proposed model and algorithm

Motivated by the TGV, we modify the TGV_α^2 and propose an adaptive image decomposition model

$$\min_u E(u) = \Psi(u) + \frac{\beta}{2} \left\| \nabla \left(\Delta^{-1} \right)(f - u) \right\|_2^2, \quad (7)$$

where $\Psi(u) = \min_{\omega \in BD(\Omega)} \alpha_1 \int_\Omega g(x) |\nabla u - \omega|\, \mathrm{d}x + \alpha_0 \|\varepsilon(\omega)\|_1$, $g(x) = \frac{1}{1+\text{K}|\nabla G_\sigma * f|^2}$ is an edge indicator function, $G_\sigma(x) = \frac{1}{2\pi\sigma^2} \exp\left(-\frac{|x|^2}{2\sigma^2}\right)$ is the Gaussian filter with parameter σ, $\text{K} \ge 0$ is the contrast factor. $BD(\Omega)$ denotes the space of vector fields of bounded deformation, that is, $\omega \in L^1(\Omega, R^d)$ such that the distributional symmetrized derivative $\varepsilon(\omega) = \frac{\nabla \omega + \nabla \omega^T}{2}$ is a $S^{d \times d}$-valued Radon measure [14]. $\alpha_1 > 0$, $\alpha_0 > 0$, $\beta > 0$ are the tuning parameters, f is the observed image.

Let us briefly mention some properties of the proposed model (7). First, when $\text{K} = 0$, then $g(x) = 1$ and $\Psi(u)$ turns into the second-order TGV. Second, $g(x)$ can better preserve the edges in the cartoon of image [16]. Finally, from the definition 1 and definition 2, we can see that $\Psi(u)$ can measure the jump of the derivatives, from the zeroth to the 1-th order, so it can reduce the staircase effect. In addition, each function of bounded variation admits a finite TGV value, which

makes the notion to be suitable for images. This means that piecewise constant images can be captured by TGV model. Compared (7) with (3), the proposed model (7) can reduce the staircase effect while decomposing image, meanwhile, it can adaptively preserve the key features such as edges, which is very important in image decomposition.

3.1 Split Bregman algorithm for the proposed model (7)

Recently, the split Bregman method has become a very effective tool for solving various inverse problems [17–20]. The method is proven to be equivalent to the augmented Lagrangian method [21] and also belongs to the framework of the Douglas-Rachford splitting algorithm [22]. With the advantages such as fast convergence speed, numerical stabilities and smaller memory footprint, etc., see details in [22]. The split Bregman method has been used widely in the image processing. In the following, we shall use it to solve the proposed model (7).

Firstly, we introduce a variable z in Eq. (7) and let $z = u$. Then we can get

$$\min_{u,z} \Psi(u) + \frac{\beta}{2} \left\| \nabla\left(\Delta^{-1}\right)(f-z) \right\|_2^2, \quad \text{s.t. } z = u. \quad (8)$$

Introducing the auxiliary variable d and using the split Bregman method, we have

$$u^{k+1} = \arg\min_u \Psi(u) + \frac{\mu}{2} \left\| u - z^k - d^k \right\|_2^2, \quad (9)$$

$$z^{k+1} = \arg\min_z \frac{\beta}{2} \int_\Omega \left| \nabla\left(\Delta^{-1}(f-z)\right) \right|^2 \mathrm{d}x$$

$$+ \frac{\mu}{2} \left\| u^{k+1} - z - d^k \right\|_2^2, \quad (10)$$

$$d^{k+1} = d^k - u^{k+1} + z^{k+1}, \quad (11)$$

3.2 Chambolle and Pock's algorithm for Eq. (9)

In this subsection, we use the Chambolle and Pock's primal-dual algorithm [23] to solve the first subproblem (9). The algorithm has been shown to be a good choice for large-scale convex optimization problems in image processing [23].

Definition 3 Assume that Ω is a Hilbert space. The dual, also called the polar, of the proper functional $\varphi : \Omega \to R \cup \{\infty\}$ is defined as

$$\varphi^* : \Omega^* \to R \cup \{\infty\}, \; \varphi^*(w^*) = \max_{w \in \Omega} \{\langle w^*, w \rangle - \varphi(w)\}. \quad (12)$$

If φ is a proper, lower-semi-continuous and convex function, we have the bi-conjugate $\varphi^{**} = \varphi$.

For Eq. (9), we first set

$$\vartheta_1 = \nabla u - \boldsymbol{\omega}, \; \vartheta_2 = \varepsilon(\boldsymbol{\omega}),$$

$$F_1(\vartheta_1) = \alpha_1 \int_\Omega g \, |\vartheta_1| \, \mathrm{d}x, \; F_2(\vartheta_2) = \alpha_0 \int_\Omega |\vartheta_2| \mathrm{d}x. \quad (13)$$

It is obvious that F_1, F_2 are both proper, lower-semi-continuous and convex functions. From the above Definition 3, for the dual variable ϑ_1^* of ϑ_1, we have

$$
\begin{aligned}
F_1^*(\vartheta_1^*) &= \max_{\vartheta_1} \langle \vartheta_1^*, \vartheta_1 \rangle - F_1(\vartheta_1) \\
&= \max_{\vartheta_1} \langle \vartheta_1^*, \vartheta_1 \rangle - \alpha_1 \int_\Omega g(x) \, |\vartheta_1| \mathrm{d}x \\
&= \begin{cases} 0, & if \; |\vartheta_1^*| \le g\alpha_1, \\ +\infty, & if \; |\vartheta_1^*| > g\alpha_1. \end{cases}
\end{aligned}
\quad (14)
$$

Similarly, for the dual variable ϑ_2^* of ϑ_2, there is

$$F_2^*(\vartheta_2^*) = \begin{cases} 0, & if \; |\vartheta_2^*| \le \alpha_0, \\ +\infty, & if \; |\vartheta_2^*| > \alpha_0. \end{cases} \quad (15)$$

From Eqs. (13)–(15) and $F_1^{**} = F_1$, $F_2^{**} = F_2$, let $\mathbf{p} = \vartheta_1^*$, $\mathbf{q} = \vartheta_2^*$, then we can get

$$
F_1^*(\boldsymbol{p}) = \begin{cases} 0, & if \; |\mathbf{p}| \le g\alpha_1, \\ +\infty, & if \; |\mathbf{p}| > g\alpha_1. \end{cases},
$$

$$
F_2^*(\mathbf{q}) = \begin{cases} 0, & if \; |\mathbf{q}| \le \alpha_0, \\ +\infty, & if \; |\mathbf{q}| > \alpha_0. \end{cases}
\quad (16)
$$

$$F_1(\nabla u - \boldsymbol{\omega}) = \max_{\mathbf{p}} \langle \nabla u - \boldsymbol{\omega}, \mathbf{p} \rangle - F_1^*(\mathbf{p}),$$

$$F_2(\varepsilon(\boldsymbol{\omega})) = \max_{\mathbf{q}} \langle \varepsilon(\boldsymbol{\omega}), \mathbf{q} \rangle - F_2^*(\mathbf{q}).$$

So Eq. (9) can be rewritten

$$
\begin{aligned}
&\arg\min_u \Psi(u) + \frac{\mu}{2} \left\| u - z^k - d^k \right\|_2^2 \\
&= \arg\min_{u, \boldsymbol{\omega}} \alpha_1 \int_\Omega g(x) |\nabla u - \boldsymbol{\omega}| \, \mathrm{d}x + \alpha_0 \| \varepsilon(\boldsymbol{\omega}) \|_1 \\
&\quad + \frac{\mu}{2} \left\| u - z^k - d^k \right\|_2^2 \\
&= \arg\min_{u, \boldsymbol{\omega}} F_1(\nabla u - \boldsymbol{\omega}) + F_2(\varepsilon(\boldsymbol{\omega})) \\
&\quad + \frac{\mu}{2} \left\| u - z^k - d^k \right\|_2^2 \\
&= \arg\min_{u, \boldsymbol{\omega}} \max_{\mathbf{p} \in P, \mathbf{q} \in Q} \langle \nabla u - \boldsymbol{\omega}, \mathbf{p} \rangle + \langle \varepsilon(\boldsymbol{\omega}), \mathbf{q} \rangle \\
&\quad + \frac{\mu}{2} \left\| u - z^k - d^k \right\|_2^2,
\end{aligned}
\quad (17)
$$

where $P = \{ \mathbf{p} = (p_1, p_2)^T \; || \mathbf{p}(x)| \le g\alpha_1 \}$,

$Q = \left\{ \mathbf{q} = \begin{pmatrix} q_{11}, q_{12} \\ q_{21}, q_{22} \end{pmatrix} \; | \| \mathbf{q} \|_\infty \le \alpha_0 \right\}.$

Applying the Chambolle and Pock's algorithm 1 in [23] to the last formula of Eq. (17), we can get the iterative schemes for Eq. (9) as follows

$$
\begin{cases}
\mathbf{p}^{k+1} = \mathrm{proj}_P \left(\mathbf{p}^k + \delta \left(\nabla \bar{u}^k - \bar{\boldsymbol{\omega}}^k \right) \right), \\
\mathbf{q}^{k+1} = \mathrm{proj}_Q \left(\mathbf{q}^k + \delta \left(\varepsilon(\bar{\boldsymbol{\omega}}^k) \right) \right), \\
u^{k+1} = \frac{\tau\mu(z^k + d^k) + u^k + \tau \mathrm{div}(\mathbf{p}^{k+1})}{1 + \tau\mu}, \\
\boldsymbol{\omega}^{k+1} = \boldsymbol{\omega}^k + \tau \left(\mathbf{p}^k + \mathrm{div}^\hbar(\mathbf{q}^{k+1}) \right), \\
\bar{u}^{k+1} = 2u^{k+1} - u^k, \\
\bar{\boldsymbol{\omega}}^{k+1} = 2\boldsymbol{\omega}^{k+1} - \boldsymbol{\omega}^k,
\end{cases}
\quad (18)
$$

Note that in the above Eq. (18), $\delta, \tau > 0$, $\mathrm{div}^\hbar$ is defined in Sect. 4 and

$$\mathrm{proj}_P \left(\tilde{\mathbf{p}}^l \right) = \frac{\tilde{\mathbf{p}}^l}{\max\left(1, |\tilde{\mathbf{p}}^l|/g\alpha_1\right)},$$

$$\mathrm{proj}_Q \left(\tilde{\mathbf{q}}^l \right) = \frac{\tilde{\mathbf{q}}^l}{\max\left(1, |\tilde{\mathbf{q}}^l|/\alpha_0\right)}.$$

3.3 Gauss-Seidel method for Eq. (10)

For the second subproblem (10), its Euler-Lagrange equation is

$$\beta(f - z) + \mu\Delta\left(z + d^k - u^{k+1}\right) = 0, \quad (19)$$

that is,

$$(\beta - \mu\Delta) z^{k+1} = \beta f - \mu\Delta\left(u^{k+1} - d^k\right). \quad (20)$$

To solve the Eq. (19), one can use several approaches such as Gauss-Seidel iteration, the gradient descent method or discrete cosine transform (DCT). Here, we use the Gauss-Seidel iteration to solve the problem. More explicitly, z^{k+1} can be attained from the following formula

$$
\begin{aligned}
z_{i,j}^{k+1} = &\frac{\mu}{\beta + 4\mu} \left(z_{i+1,j}^k + z_{i-1,j}^k + z_{i,j+1}^k + z_{i,j-1}^k \right. \\
&\left. -\rho_{1,i-1,j}^k + \rho_{1,i,j}^k - \rho_{2,i,j-1}^k + \rho_{2,i,j}^k \right) + \frac{\beta}{\beta + 4\mu} f_{i,j}
\end{aligned}
\quad (21)
$$

where $\rho_1 = \partial_x^+ \left(u^{k+1} - d^k \right), \rho_2 = \partial_y^+ \left(u^{k+1} - d^k \right), \partial_x^+, \partial_y^+$ denote the first-order forward difference operators of the directions x and y, respectively.

In summary, the complete algorithm for solving the model (7) can be described as follows

---

Algorithm 1. Split Bregman algorithm for Eq. (7)

- **Initialization:** $u^0, z^0, d^0, \quad k = 0$;
- **Step 1:** Compute u^{k+1} by (18);
- **Step 2:** Compute z^{k+1} by (21);
- **Step 3:** Compute d^{k+1} by the iterative formula
  $d^{k+1} = d^k - u^{k+1} + z^{k+1}$;
- $k \leftarrow k + 1$;
- **Until:** $\| u^{k+1} - u^k \|_2^2 / \| u^k \|_2^2 \le C$; otherwise return to step 1.

Fig. 1 Comparison of denoising results from three different models using "Lena" image. **a** Original image, **b** Noisy image, **c** u by OSV model, **d** u by the model in [9], **e** u by our model, **f** Local zoom of u, OSV model, **g** Local zoom of u, the model in [9], **h** Local zoom of u, our model
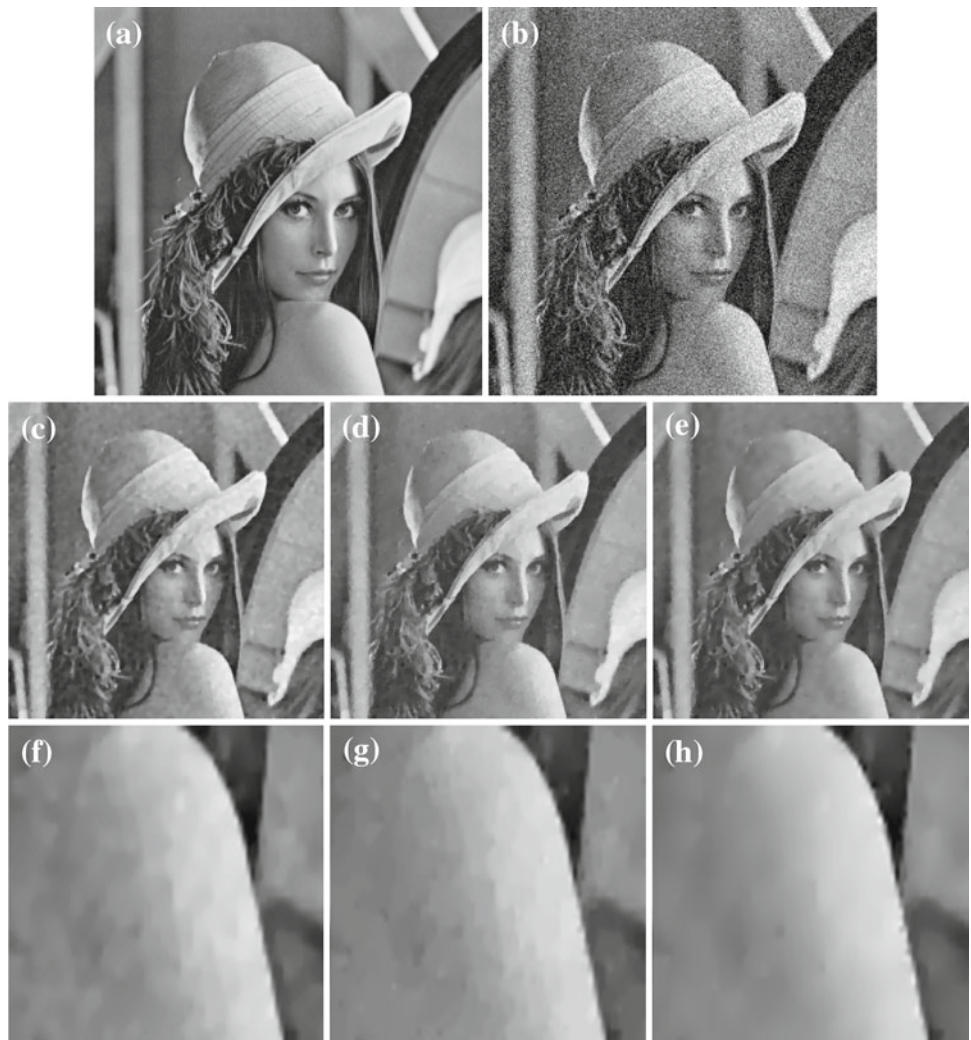
4 Numerical discretisation

In order to implement the proposed algorithm 1 on a digital computer, some discrete notations need to be introduced. For simplicity, we let the image domain be square of size $m \times n$ and the vector $\boldsymbol{\omega} = (\omega_1, \omega_2)^T$. The first-order forward and backward difference operators are, respectively, defined as

$$\left(\partial_x^+ u\right)_{i,j} = \begin{cases} u_{i+1,j} - u_{i,j}, & \text{if } 1 \leq i < m, \\ 0, & \text{if } i = m, \end{cases},$$

$$\left(\partial_y^+ u\right)_{i,j} = \begin{cases} u_{i,j+1} - u_{i,j}, & \text{if } 1 \leq j < n, \\ 0, & \text{if } j = n. \end{cases}$$

$$\left(\partial_x^- u\right)_{i,j} = \begin{cases} u_{i,j} - u_{i-1,j}, & \text{if } 1 < i < m, \\ u_{1,j}, & \text{if } i = 1, \\ -u_{m-1,j}, & \text{if } i = m, \end{cases}$$ (22)

$$\left(\partial_y^- u\right)_{i,j} = \begin{cases} u_{i,j} - u_{i,j-1}, & \text{if } 1 < j < n, \\ u_{i,1}, & \text{if } j = 1, \\ -u_{i,n-1}, & \text{if } j = n. \end{cases}$$

The gradient operator $\nabla = \left(\partial_x^+, \partial_y^+\right)^T$, and the divergence operator $\text{div} = -\nabla^*$ is defined by $\text{div}(p_1, p_2) = \partial_x^- p_1 + \partial_y^- p_2$, where ∇^* is the adjoint operator of ∇. The discrete version of the symmetric gradient operator is

$$\varepsilon(\boldsymbol{\omega}) = \frac{1}{2}\left(\nabla\boldsymbol{\omega} + \nabla\boldsymbol{\omega}^T\right)$$

$$= \begin{pmatrix} \partial_x^+ \omega_1, & \frac{1}{2}\left(\partial_y^+ \omega_1 + \partial_x^+ \omega_2\right) \\ \frac{1}{2}\left(\partial_x^+ \omega_2 + \partial_y^+ \omega_1\right), & \partial_y^+ \omega_2 \end{pmatrix}.$$ (23)

If set $\text{div}^\hbar = -\varepsilon^*$, where ε^* denotes the adjoint operator of ε, and let $\mathbf{q} = \begin{pmatrix} q_{11}, q_{12} \\ q_{21}, q_{22} \end{pmatrix}$, then we have $\text{div}^\hbar(\mathbf{q}) = \begin{pmatrix} \partial_x^- q_{11} + \partial_y^- q_{12} \\ \partial_x^- q_{21} + \partial_y^- q_{22} \end{pmatrix}.$

Fig. 2 **a** Original image, **b** noisy image, **c** cartoon component u of OSV model ($\gamma = 0.05$), **d** $f - u$ of OSV model, **e** cartoon component u of the model in [5], **f** $f - u$ of the model in [5], **g** cartoon component u of our model, **h** $f - u$ of our model, **i** local zoom of u, OSV model, **j** local zoom of u, the model in [5], **k** local zoom of u, our model


5 Numerical experiments

In this section, we demonstrate the performance of our proposed model for image denoising and decomposition. The numerical results are compared with those obtained by the OSV model, the models in [5] and [9], respectively. We use

"Lena" (256×256), "Barbara" (400×393) and the synthetic image (171×179) as the test images. In order to measure the quality of restored images, peak signal to noise ratio (PSNR), mean absolute-deviation error (MAE) [24] and structural similarity (SSIM) [25] are employed. Moreover, in all our experiments, the parameters in the edge indicator function

Fig. 2 continued
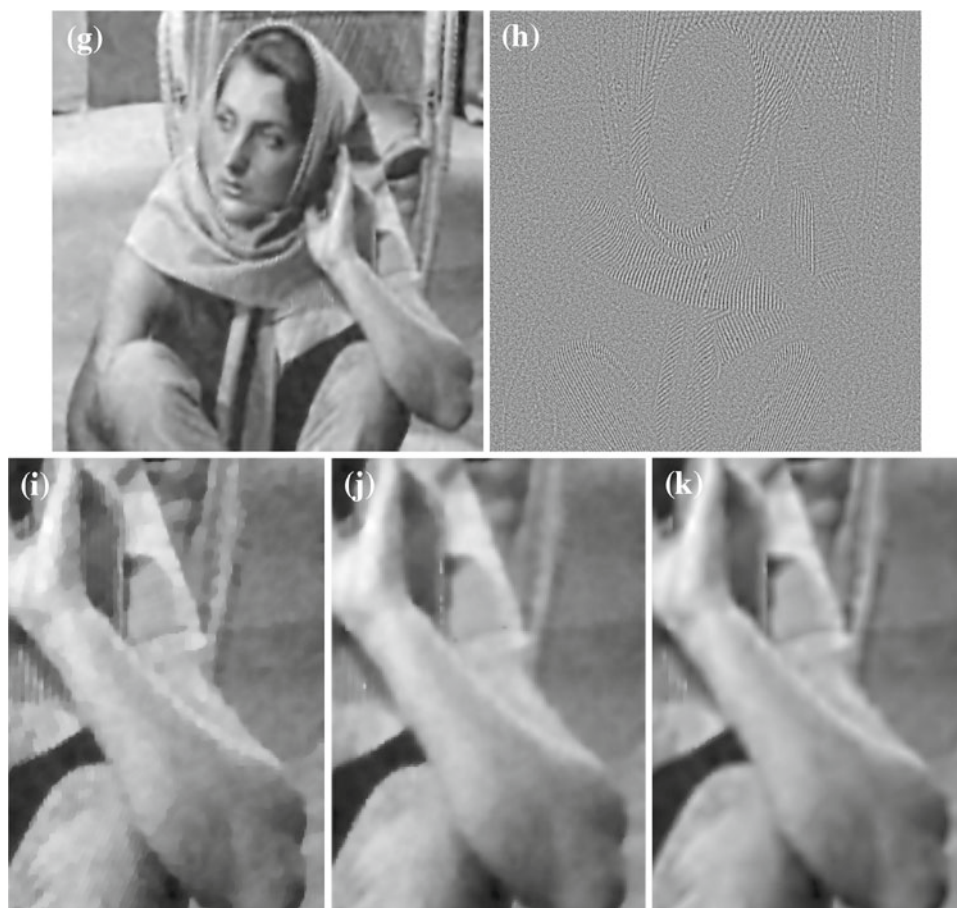
are chosen K $= 0.001$, $\sigma = 1$, and the parameter in the stopping criterion $C = 3 \times 10^{-4}$.

Experiment 1 We take the "Lena" image (256×256) for denoising test. "Lena" image is corrupted with Gaussian white noise and the noise standard deviation is 20. The parameters in our algorithm are chosen $\alpha_1 = 5$, $\alpha_0 = 5$, $\beta = 0.2$, $\mu = 0.01$, respectively. Figure 1 has given the experimental results. From the restored images and their corresponding magnifying results in Fig. 1, it is clear to see that the OSV model and the model in [9] produce obvious staircasing effect. But, for our model as expected, the smooth regions are well processed and the staircasing effect is successfully avoided while removing the noise, which makes the cartoon part restored by our model to look more natural than other two models. Moreover, the related data in Table 1. also demonstrate that the proposed model is more effective.

Experiment 2 We take the "Barbara" image (400×393) with Gaussian white noise for decomposition experiment. The noise standard deviation is 20. The parameters in the proposed algorithm are chosen to be $\alpha_1 = 10$, $\alpha_0 = 5$, $\beta = 0.2$, $\mu = 0.01$. The experiment results are shown in Fig. 2. From these results, it is not difficult to find that the staircasing

**Table 1** PSNR, MAE, SSIM for different models in experiment 1

Model	PSNR	MAE	SSIM
OSV	28.9803	6.5554	0.8172
[9]	29.2727	6.2418	0.8342
Ours	**29.4190**	**6.0417**	**0.8470**

The best value of each column is highlighted in bold

effect appears in the cartoon component u of the OSV model, which can be seen clearly in Fig. 2i. Though the model in [5] can reduce the staircasing effect, the cartoon part has become blurry and there are some speckle pixels. Compared with the OSV model, The proposed model cannot only avoid the staircasing effect in the cartoon component u which can be seen clearly from Fig. 2k, but also extract the texture components successfully from the observed image with very few structural features. Furthermore, Compared with the model in [5], the cartoon component u of our model looks more natural and clear. So our proposed method can achieve a better trade-off between the noise removal and image decomposition, while avoiding the staircasing effect effectively.

Experiment 3 We consider the clean synthetic image (171×179) for the cartoon + texture decomposition test. In the

Fig. 3 **a** Original image,
b cartoon component of OSV
model ($\gamma = 0.05$), **c** texture
component of OSV model,
d cartoon component of our
model, **e** texture component of
our model
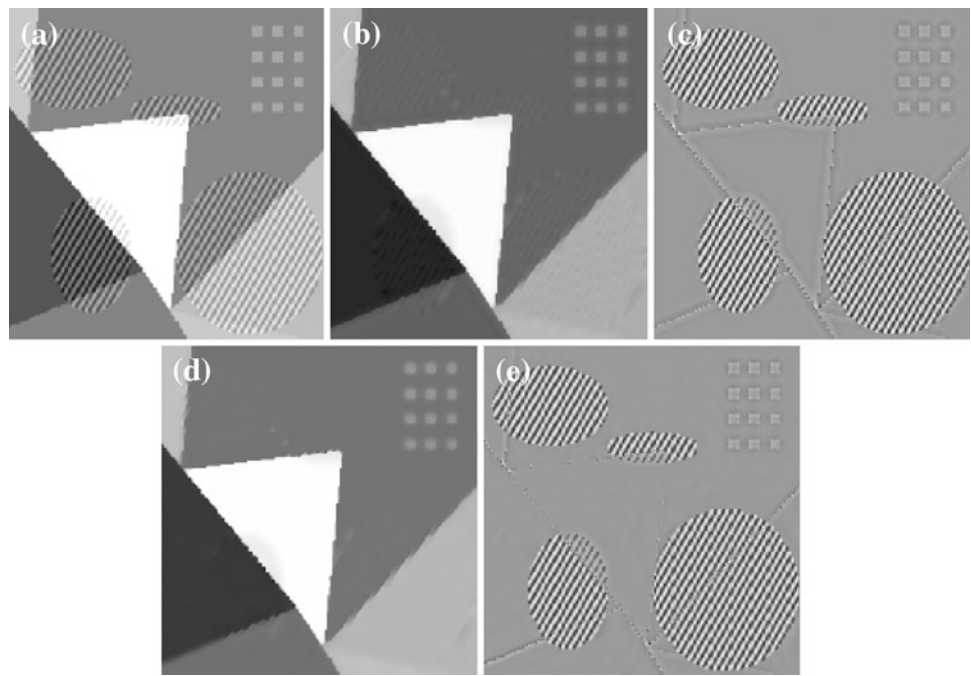
experiment, the parameters in our proposed algorithm are chosen to be $\alpha_1 = 5$, $\alpha_0 = 5$, $\beta = 0.2$, $\mu = 0.01$. Figure 3 give the decomposition results of the synthetic image. From which we can easily find that the edges are retained successfully in cartoon component by our proposed model. These can be clearly seen from Fig. 3e, such as the edges of triangle in Fig. 3e. Moreover, by comparing the Fig. 3b, d, we can also clearly see that the textures are extracted better by our proposed model, and there are some textures are not yet extracted out from the cartoon components by the OSV model.

6 Conclusions

In this paper, we propose a new variational model for image decomposition by adaptive TGV regularizer. Compared with the OSV model based on TV regularizer, the proposed model cannot only preserve the key features such as object boundaries while avoiding staircasing, but also can well extract the texture. In addition, To solve the proposed model, the split Bregman method and primal-dual approach are used in the numerical algorithm. The numerical experiments show that the proposed model is more effective for image decomposition.

References

1. Meyer, Y.: Oscillating patterns in image processing and nonlinear evolution equations. University Lecture Series, American Mathematical Society, Boston (2001)
2. Rudin, L., Osher, S., Fatemi, E.: Nonlinear total variation based noise removal algorithms. Physica. D **60**, 259–268 (1992)
3. Vese, L., Osher, S.: Modeling textures with total variation minimization and oscillating patterns in image processing. J. Math. Imaging Vis. **20**, 7–18 (2004)
4. Osher, S., Sole, A., Vese, L.: Image decomposition and restoration using total variation minimization and the H^{-1} norm. Multiscale Model. Simul. **1**(3), 349–370 (2003)
5. Jiang, L., Yin, H., Feng, X.: Adaptive variational models for image decomposition combining staircase reduction and texture extraction. J. Syst. Eng. Electron. **20**(2), 254–259 (2009)
6. Chan, T.F., Esedoglu, S.F., Parky, E.: Image decomposition combining staircase reduction and texture extraction. J. Vis. Commun. Image Represent. **18**(6), 464–486 (2007)
7. Aujol, J.F., Chambolle, A.: Dual norms and image decomposition models. Intl. J. Comp. Vis. **63**(1), 85–104 (2005)
8. Duval, V., Aujol, J.F., Vese, L.: Mathematical modeling of textures: Application to color image decomposition with a projected gradient algorithm. J. Math. Imaging Vis. **37**(3), 232–248 (2010)
9. Bai, J., Feng, X.: Image denoising and decomposition using non-convex functional. Chinese J. Electron. **21**(1), 102–106 (2012)
10. Jiang, L., Feng, X., Yin, H.: Image decomposition using optimally sparse representations and a variational approach. Signal, Image and Video Processing **22**(4), 1287–1292 (2007)
11. Starck, J., Elad, M., Donoho, D.: Image decomposition via the combination of sparse representations and a variational approach. IEEE Trans. Image Process. **14**(10), 1570–1582 (2005)
12. Bredies, K., Kunisch, K., Pock, T.: Total generalized variation. SIAM J. Imaging Sci. **3**(3), 492–526 (2010)
13. Bredies, K., Valkonen, T.: Inverse problems with second-order total generalized variation constraints. In: Proceedings of SampTA

2011–9th International Conference on Sampling Theory and Applications, Singapore, pp. 1–4 (2011)

14. Bredies, K., Dong, Y., Hintermüller M.: Spatially dependent regularization parameter selection in total generalized variation models for image restoration. International Journal of Computer Mathematics, pp. 1–15 (2012), online, doi:10.1080/00207160.2012.700400

15. Knoll, F., Bredies, K., Pock, T., Stollberger, R.: Second order total generalized variation (TGV) for MRI. Magn. Res. Med. **65**(2), 480–491 (2011)

16. Dong, F., Liu, Z., Kong, D., Liu, K.: An improved LOT model for image restoration. J. Math. Imaging Vis. **34**(1), 89–97 (2009)

17. Goldstein, T., Osher, S.: The split Bregman method for L1 regularized problems. SIAM J. Imaging Sci. **2**(2), 323–343 (2009)

18. Han, Y., Wang, W., Feng, X.: A new fast multiphase image segmentation algorithm based on nonconvex regularizer. Pattern Recongnit. **3**(4), 363–372 (2012)

19. Goldstein, T., Bresson, X., Osher, S.: Geometric applications of the split Bregman method: Segmentation and surface reconstruction. J. Sci. Comput. **45**(1–3), 272–293 (2010)

20. Afonso, M., Bioucas-Dias, J., Figueiredo, M.: An augmented lagrangian approach to the constrained optimization formulation of imaging inverse problems. IEEE Trans. Image Process. **20**(3), 681–695 (2011)

21. Wu, C., Tai, X.C.: Augmented Lagrangian method, dual methods and split-Bregman iterations for ROF, vectorial TV and higher order models. SIAM J. Imaging Sci. **3**(3), 300–339 (2010)

22. Setzer, S.: Operator splittings, Bregman methods and frame shrinkage in image processing. Int. J. Comput. Vision **92**(3), 265–280 (2011)

23. Chambolle, A., Pock, T.: A first-order primal-dual algorithm for convex problems with applications to imaging. J. Math. Imaging Vis. **40**(1), 120–145 (2011)

24. Hao, Y., Feng, X.C., Xu, J.L.: Multiplicative noise removal via sparse and redundant representations over learned dictionaries and total variation. Signal Process. **92**(6), 1536–1549 (2012)

25. Wang, Z., Bovik, A., Sheikh, H., Simoncelli, E.: Image quality assessment: From error visibility to structural similarity. IEEE Trans. Image Process. **13**(4), 1–14 (2004)